The application of silver oxide thin films to plasmon photonic devices

2003 J. Phys.: Condens. Matter 15 R1101

(http://iopscience.iop.org/0953-8984/15/25/201)

INSTITUTE OF PHYSICS PUBLISHING JOURNAL OF PHYSICS: CONDENSED MATTER

J. Phys.: Condens. Matter **15** (2003) R1101–R1122 PII: S0953-8984(03)34844-1

TOPICAL REVIEW

The application of silver oxide thin films to plasmon photonic devices

Junji Tominaga

Centre for Applied Near-Field Optics Research (CAN-FOR), National Institute of Advanced Industrial Science and Technology (AIST), 1-1-1 Higashi, Tsukuba 305-8562, Japan

E-mail: j-tominaga@aist.go.jp

Received 6 January 2003
Published 13 June 2003
Online at stacks.iop.org/JPhysCM/15/R1101

Abstract

Silver has long been used for mirrors and tableware due to its high reflectivity, and it is still a very important component in optics. In particular, silver island films or small particles have been applied as photographic materials, tools and devices to generate localized electrical fields for molecular detection and electrical field enhancement.

It has recently been discovered that silver oxide thin films may be a very useful material for dealing with optical near-field and surface plasmons. Silver oxide decomposes into oxygen and small metallic silver particles, and this characteristic has been applied to ultrahigh-density optical data storage to create a strong light-scattering centre that resolves small pits or marks beyond the diffraction limit. More recently, it has been found that silver film can be cheaply and easily transformed into Ag nanoparticles and nanowires in a gas mixture of hydrogen and oxygen in a vacuum chamber. The particle and wire diameters are very uniform and approximately 20–50 nm, and they can be three-dimensionally fabricated on almost all material surfaces without the need for thermal annealing. Silver nanoparticles and wires will soon appear in small and cheap molecular detection sensors by small precise adjustments for generating surface plasmon conditions.

Contents

1. Introduction and background to silver plasmon devices

Silver is one of the most promising materials for plasmon science and engineering because of its unique characteristics of high reflectivity and electrical conductivity. The island structures deposited by vacuum techniques on several substrates and the colloid oxides synthesized from aqueous solutions have been widely used for generating surface plasmons and achieving electrical–magnetic field enhancement for Raman spectroscopy [1–12]. Surface plasmon polaritons have recently attracted more attention in the fields of application devices combined with biotechnology and single-molecular science [13–16]. For example, by depositing a silver thin film on a thin glass substrate placed on a prism, small amounts of chemicals or molecules can be detected with good accuracy. In this type of system, attenuated total reflection (ATR), otherwise known as *Kretschman geometry*, is typically adapted for the objectives [17, 18]. An incident laser beam is introduced into the prism and totally reflected at the bottom surface. Surface plasmon polaritons (hereafter abbreviated to SPs) are then stimulated on the surface of the Ag thin film. While orienting the incident beam angle to the bottom surface, it is observed that the reflected power drops suddenly in a specific narrow region of the angle, which depends on the beam wavelength and refractive indices of the film and surrounding medium [18]. The excitation condition of SP is easily derived from Maxwell's equations with two media: one is a semi-infinite metal (medium 1) with a dielectric constant of $\varepsilon_1 = \varepsilon_1' + \mathrm{i}\varepsilon_1''$ and the other a dielectric medium (medium 2) with ε_2 such as air or a vacuum. In two dimensions, a wavevector k_{z2} (far-field light) in medium 2 has to satisfy the condition

$$k_{z2} = [\varepsilon_2(\omega/c)^2 - k_x^2]^{1/2}. \tag{1}$$

Here, k_x is the wavevector (evanescent wave) that sweeps along the interface of the two media, which must be the same in both media. Using a dispersion relation, $k_{z1}/\varepsilon_1 + k_{z2}/\varepsilon_2 = 0$, we can eliminate k_{zi} $(i = 1, 2)$ from equation (1), allowing the dispersion relation to be more simply given as

$$k_x = \omega/c[\varepsilon_1\varepsilon_2/(\varepsilon_1 + \varepsilon_2)]^{1/2}. \tag{2}$$

In metals, the dielectric constant ε_1 is imaginary. The satisfying condition for being a real k_x is $\varepsilon_{1(\mathrm{Real})} < 0$ and $|\varepsilon_{1(\mathrm{Real})}| > \varepsilon_2$. According to this condition, equation (1) may become imaginary while the incident light wave is sweeping along the interface. The electrical wave is SP. An ATR using a prism is one of the simplest and most easily constructed devices that satisfies the condition (see figure 1). Alternative methods of generating SPs besides ATR are to use corrugated or periodic gratings and surface roughness [13, 18–20]. When using corrugation and surface roughness it is especially difficult to control the generation position of SR, since it depends on coincidence. Such SPs have been widely observed and reported thanks to the development of the *scanning near-field optical microscope (SNOM)*. The periodic grating is therefore more interesting and useful for future SP devices, thanks to nanotechnologies that enable the fabrication of photonic crystals and other photonic devices [21, 22].

Related to SP on thin-film metals, on the other hand, is *surface-enhanced Raman spectroscopy (SERS)*, of great interest because of its very strong electromagnetic field enhancement. Since the first discovery of SERS using a silver electrode, a huge number of SERS studies have been reported, especially in solutions with metal electrodes and metal

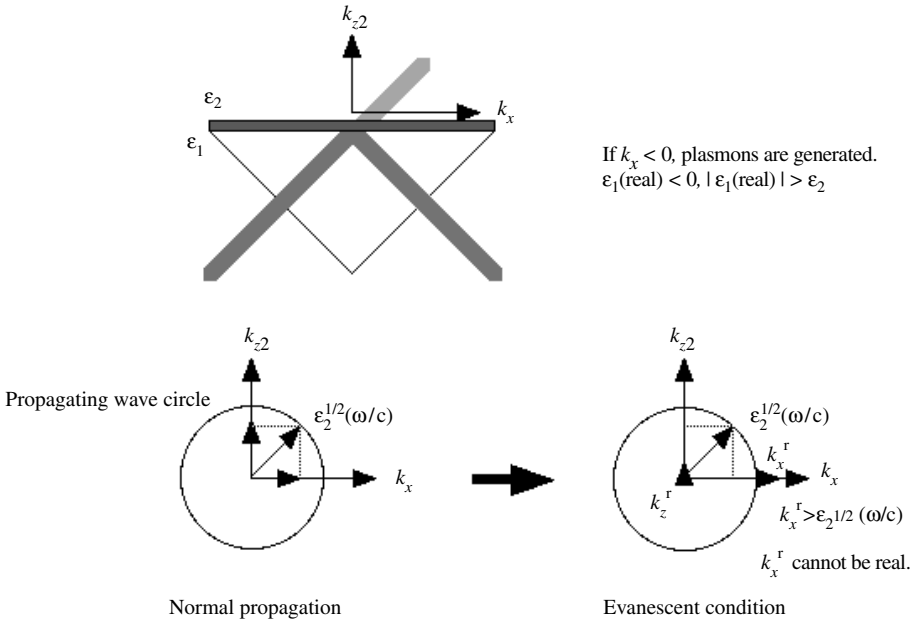

Figure 1. Schematic picture of ATR and an image symbolically explaining the relationship between a far-field propagating wave (k_z) and an evanescent wave $k_{x'}$. Under normal conditions, k_z and k_x cannot exist beyond the propagating wave circle; however, using an ATR device or grating under evanescent conditions, an additional k_x is generated, and the total vector is able to escape the circle. The result is that k_z is no longer real and an SP is generated at the medium's interface.

colloids [5–9]. SERS characteristics at first glance appear to be related to SP, but it soon becomes clear that the characteristics have similar features of *localized surface plasmons (LSP)* with corrugations and protrusions on a metal surface. Several papers and reports are very helpful in understanding the field enhancement at a metal-coated protrusion or atomic-force microscope tip [23–27]. When focusing a laser beam on such a tip or protrusion, a strong electrical field is generated. SERS effects were recently confirmed by Inouye *et al* [24, 25]. Although the origin of SERS is not fully understood, it has gradually become clear that the strong accumulated and concentrated electrical field at a very small localized spot (hot spot) plays a major role in acting as the source of SERS [5, 10].

In this review paper, we focus on silver oxide (AgO_x) thin film as an SP and SERS source. We describe the unique features and transitions of the film and its very promising potential applications to novel photonic devices in the near future.

2. The characteristics of silver oxide thin films

The first ever synthesis of AgO_x thin film has not been elucidated; however, it was assumed to be formed in an electrochemical process. Up to now, AgO_x thin films have usually been produced by chemical reaction between $AgNO_3$ and NaOH to produce colloidal AgO_x [5, 16]. The obtained colloids are dispersed or spin-coated on a substrate and finally dried to remove the solvent. In this type of aqueous or 'wet' reaction, the composition ratio of oxygen to the total is not controlled, and early studies of the AgO_x focused on investigating its structural analysis and chemical bonding properties. In 1991, one paper related to the application of a

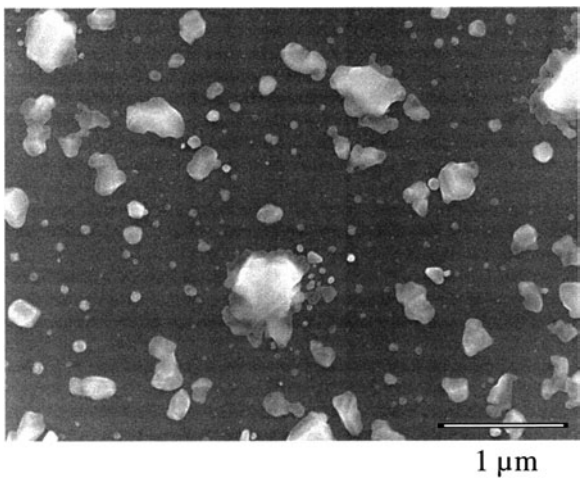

Figure 2. SEM picture of Ag particles thermally decomposed from AgO film. The film temperature was raised to 450 °C at a temperature ramp rate of 30 °C min^{-1}. The substrate was Si [30] in optical storage and optical information processing.

thin film of AgO_x to optical data storage was published, and the synthesis of AgO_x thin films using a dry process was first reported using RF-reactive sputtering with a Ag target and a gas mixture of Ar and O_2 [28, 29]. In the data storage application, a *nano-explosion* induced by local thermal decomposition of the AgO_x thin film (60–70 nm thick) was applied to fabricate a submicron-sized bubble as a recording pit in a compact disc. In the paper, the refractive indices obtained by sputtering gas composition were first reported but with low accuracy. Since then, the dry process, and the thermal and optical properties of the films, have gradually been closely examined, especially for their potential as recording materials with high-density optical data storage [30, 31].

In the initial application of the AgO_x thin films, SPs were ignored, and the thermal decomposition of the film into Ag and oxygen was used only to generate submicron-sized oxygen gas bubbles [28, 29]. As is well known in chemistry, the binding energies of bulk AgO_x are very low: it gradually decomposes at a temperature of 160 °C, leaving silver islands on the substrate (see figure 2).

The AgO_x thin films sputtered by RF reactive sputtering show mostly the same characteristics as those of the bulk material [32]. The light transmittances of films produced at different gas mixture ratios of O_2 to the total (Ar + O_2) (here, the mixture means the gas flow ratio, not the partial pressure) are shown in figure 3.

It is clearly found that at a lower oxygen ratio, the transmittance of light decreases only to a small degree at 160 °C, then steeply decreases as a result of thermal decomposition. In contrast, in films produced under more O_2-rich conditions, the transmittance first increases up to the threshold temperature, and then decreases. This behaviour depends entirely on the O_2 gas flow ratio during the deposition process. The refractive index change of the deposited films against the O_2 gas flow ratio is displayed in figure 4 [30]. The real index increases steeply and becomes saturated at 2.6 at a ratio of more than 0.3, while the imaginary index first drops rapidly to 0.1 at a ratio between 0.4 and 0.6, and then increases up to 1.5 under increasingly O_2-rich conditions. According to the experimental results, it is possible to categorize the AgO_x film compositions into three phases: phase I is a silver-rich composition with a ratio less than 0.2; phase II consists mostly of Ag_2O (at around 0.25); phase III is a mixed phase of

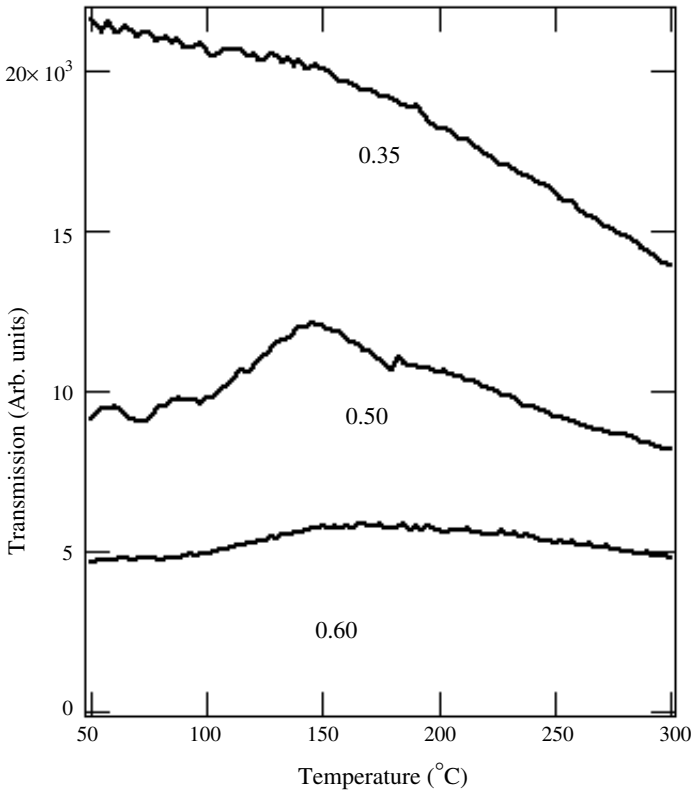

Figure 3. Light transmission of AgO_x films. 0.35, 0.50 and 0.60 refer to the O_2 gas flow ratios to the total gas mixture with Ar. The film thickness was fixed at 100 nm. The temperature ramp rate was 30 °C min^{-1} [30].

Ag_2O and AgO (more than 0.3). Phase III is an unstable phase that decomposes into Ag_2O and O_2 even at temperatures below the threshold, as shown in figure 3. The colour of the film is dark brown. Phase II is the most stable phase, and is transparent but slightly grey. The unique behaviour in the light transmittance of the O_2-rich AgO_x film is therefore due to the thermal decomposition of the AgO to Ag_2O [33, 34].

3. SERS and molecular detection device with AgO_x films

As has been mentioned above, SERS may be one of the most promising research fields for application of AgO_x thin films to *LSP* devices. Up to now, a large amount of research with SERS has been done using silver oxides prepared through wet processes, after which enhanced Raman spectra, including very strong fluorescence and light sparkles, have been observed. Moreover, SERS has recently been applied to detect single molecules. However, the colloid layer and island-like metallic film are not uniform on the nanometre scale, and the characteristics emerging from the hot spots appear and disappear at random. Although SERS is an interesting study for physicists and chemists, unfortunately its potential application as an analytical tool appears poor.

Very recently, a SERS application using a dry-processed AgO_x thin film was proposed for the first time by Büchel *et al* [35]. They observed very strong and high SERS spectra of benzoic

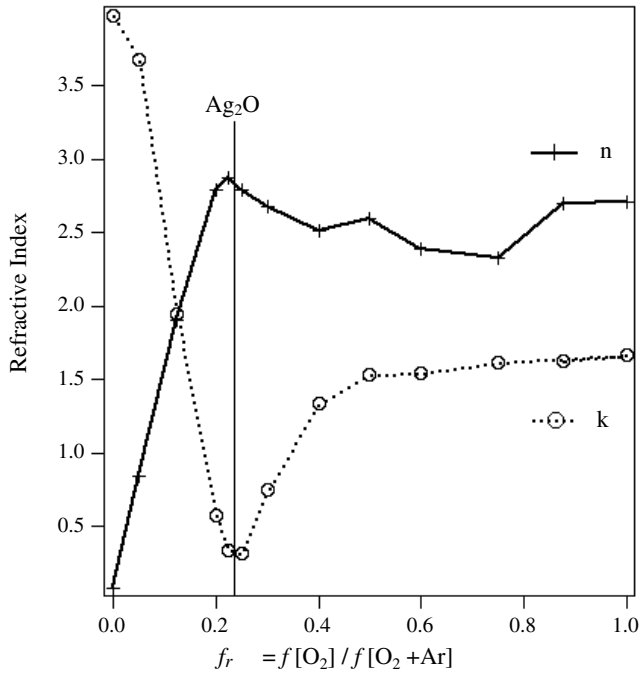

Figure 4. Refractive indices of reactive RF-sputtered AgO_x films. f refers to O_2 gas flow ratio to the total.

acid (BA) molecules in 2-propanol solution (10^{-4} M) with fluorescence and sparkles, using only a film thickness of 15 nm. As shown in figure 5, the experimental set-up is very simple: an AgO_x film is deposited at an O_2 gas flow ratio of 0.75 and then dipped in the solution; a 488 nm laser beam is then focused onto the film surface to obtain the Raman spectra. A beam focused using an objective lens (NA 0.6 or higher in our experiment) generates heat on the sample surface, resulting in the creation of hot spots due to rapid AgO_x decomposition. Raman spectra of 2-propanol are soon dominated by the BA spectra, even if the solution is diluted to less than 10^{-8} M (figure 6).

SERS observations with dry-processed AgO_x films are highly reproducible and stable, so they clearly have potential as molecular sensors. The greatest advantage of the *LSP* device using the AgO_x thin films over any other SP sensors is that complicated optical components and alignments are no longer needed. Focusing the laser beam and adjusting the power decomposes the film into Ag particles, which play a role in generating such strong *LSPs* for the SERS.

The nanometre-scale view of a hot spot with the strong SERS on the AgO_x thin film is very interesting. The source of electromagnetic field enhancement by the incident laser beam must remain. Figure 7(a) shows the active SERS area observed using a scanning electron microscope (SEM). As expected, nanometre-size Ag particles are left in the central region, and amazingly large numbers of Ag nanowires are also generated around the hot spot. Although the mechanism of formation of these nanowires is not yet known, it must be understood that the strong SERS origin is due to the electromagnetic field enhancement generated by these Ag nanoparticles and nanowires.

The potential application of the SERS active AgO_x thin films to molecular sensors is very intriguing and hopeful, since the film is self-active for *LSP* without any ATR conditions

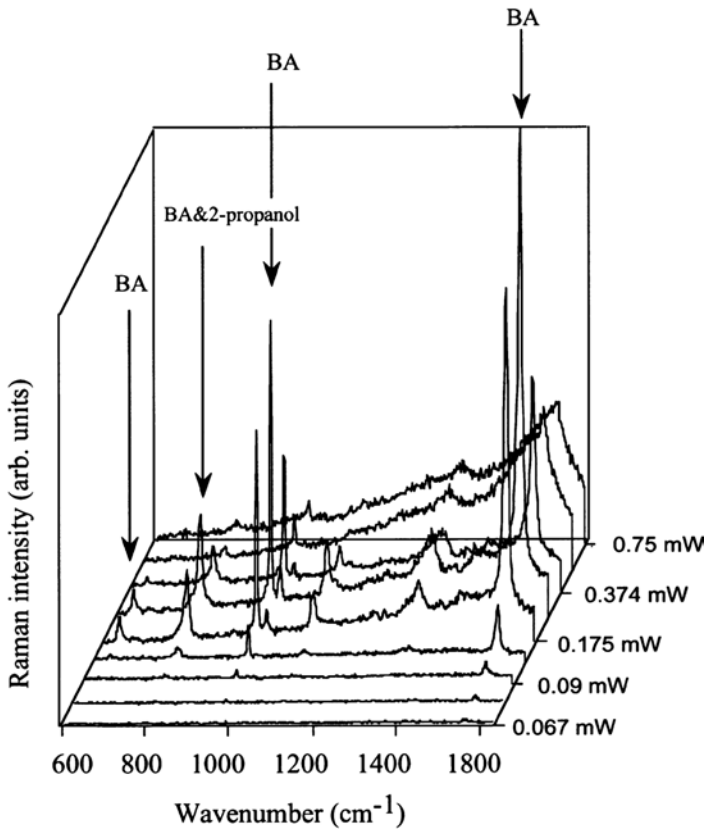

Figure 5. Typical Raman spectra of BA in 2-propanol solution (10^{-4} M). At low laser power of less than 0.1 mW, only the spectra of 2-propanol were observed. With increasing power, BA spectra were more clearly observed and the 2-propanol spectra were suppressed. At more than 0.2 mW, the BA spectra gradually disappeared. The laser wavelength for the Raman measurement was 488 nm.

using a prism. Although the detailed mechanism has not been clarified, Dickson *et al* [16] recently reported on single-molecule detection by an AgO_x film which was not produced by a dry process, but a wet one. One the other hand, Mihalcea *et al* [36] performed a series of SERS experiments on AgO_x thin films using different solutes. One of the most interesting properties of SERS activity using AgO_x films, in addition to the strong fluorescence, is that the film plays the role of an acid with respect to solutes in a 2-propanol solution. In other words, the film can select the SERS spectrum of the strongest base in a mixed solution. This is due to the affinity between active Ag^+ on the film and the basicity of the solute molecules. In the series of experiments by Mihalcea *et al*, it should be noticed that the huge and selective SERS activity can be manifested by simply focusing a laser beam on the film surface. No other special techniques are needed. When used with currently commercialized bio-sensors for fluorescent detection, AgO_x films will not only strengthen the functions of detection systems, but also enable the further miniaturization of the cell, since the SERS is generated between Ag nanoparticles.

Silver nanowires generated as by-products in the active SERS using AgO_x films are also interesting from the physical and technological viewpoints. At the moment, although the mechanism of formation is little understood, there is great potential to produce a large quantity

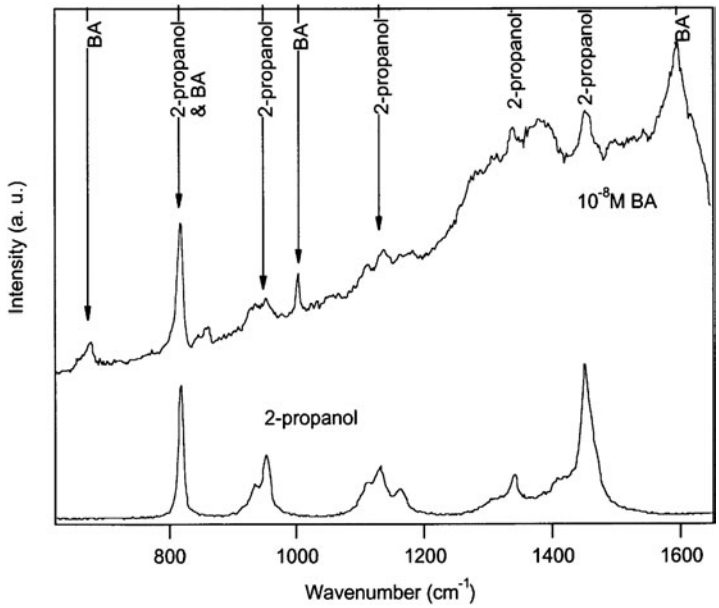

Figure 6. BA Raman spectra of 10^{-8} M (up) and the 2-propanol spectra in comparison (down).

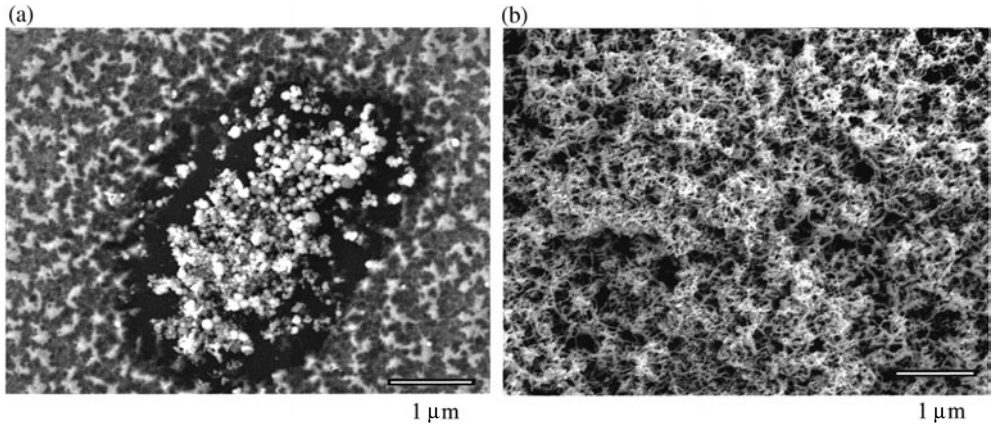

Figure 7. SEM images of a Raman hot spot. (a) Small Ag particles are confirmed to be present at the focused region of the incident laser. The size range is approximately 20–100 nm. (b) Ag nanowires surround the hot spot (a). The nanowire diameter is about 20–30 nm.

of Ag nanowires continuously with AgO_x films. Future integrated circuits with dimensions of under 100 nm will be able to incorporate Ag nanowires as electrodes and connections. Scanning a laser beam spot from one point to another in a solution such as that used in a SERS will induce an electrical nanowire to form as a bridge between them. In this process, the heat damage would be minimal and restricted to a much smaller region than that required to produce carbon nanotubes (CNTs) as bridges, since the AgO_x decomposition temperature is much lower (160 °C) than in the production of CNTs. In the wet process with a focused laser beam on the film, however, the nanowire production yield will not be significantly improved. Alternative ways are urgently needed, such as by the application of dry processes.

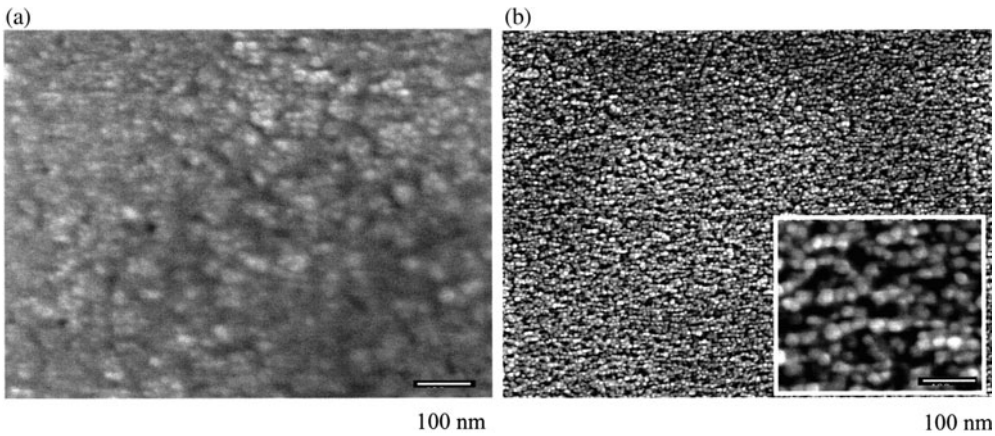

Figure 8. (a) SEM image of AgO_x film surface before deoxidation, and (b) Ag nanoparticles generated after 5 min deoxidation with a gas mixture of H_2 and O_2. Inset is an expanded image.

4. Transformation of AgO_x into Ag nanostructured films

Very recently, we proposed a simple method for transforming AgO_x films into Ag nanoparticles or nanowires [37]. The method is based on the deoxidization of AgO_x film in a H_2 atmosphere. However, if the film is irradiated under a pure H_2 plasma, the film is spontaneously deoxidized, resulting in a uniform Ag thin film without any nanostructures. In order to control and modify the deoxidation speed, a gas mixture with added oxygen gas is effective for dilution; however, it remains only a help. Instead, the deoxidized Ag film shows precursors of nanostructures whose sizes are not uniform and are in the range of 50–100 nm even under redox conditions. With further reduction of the size of the redox film, some type of catalyst or seed would need to be introduced into the process to act as nuclei for the nanostructures. After careful study and experimentation, we discovered that a small amount of CF_4 is able to seed nanostructures with much smaller dimensions. Before deoxidation, the reactive ion etching chamber is first activated by CF_4 plasma for approximately 1–5 min. If the activation time is extended, more deoxidation time is needed. For example, for 1 min activation, the following deoxidation time is approximately 2–5 min; for 5 min activation, it takes more than 40 min to obtain the same structured surface. Figure 8(a) shows a SEM image of an as-deposited AgO_x film surface. The surface is not clear: it has small grains of different sizes. However, Ag nanoparticles are generated by 5 min deoxidation, as shown in figure 8 (b). Amazingly, each particle size is very uniform and approximately 20 nm, and the whole sample surface is covered with these Ag nanostructures. It is very important to note that in this process thermal treatment is no longer needed; this means that any substrate, including dielectrics, metals, plastics etc, can be used.

Additionally, it should be mentioned that the Ag nanoparticles are generated via nanowires as the precursor. As mentioned before, concerning the role of CF_4 activation, seeds for the nanostructures are generated on parts of the AgO_x surface by the chemical reaction between AgO and fragments of CF_4, although we doubted that AgF acted as the seeds. The unseeded areas are heavily deoxidized, with most of the oxygen removed. The remaining Ag has a relatively high mobility and moves to the seed to take part in particle growth; however, as half of the nuclear surface is covered with AgF, the deoxidized Ag can be transported only from the bottom to the surface layer. As a result, the nanowires grow only on the surface. However, it is not yet understood why the nanowires are further transformed into nanoparticles.

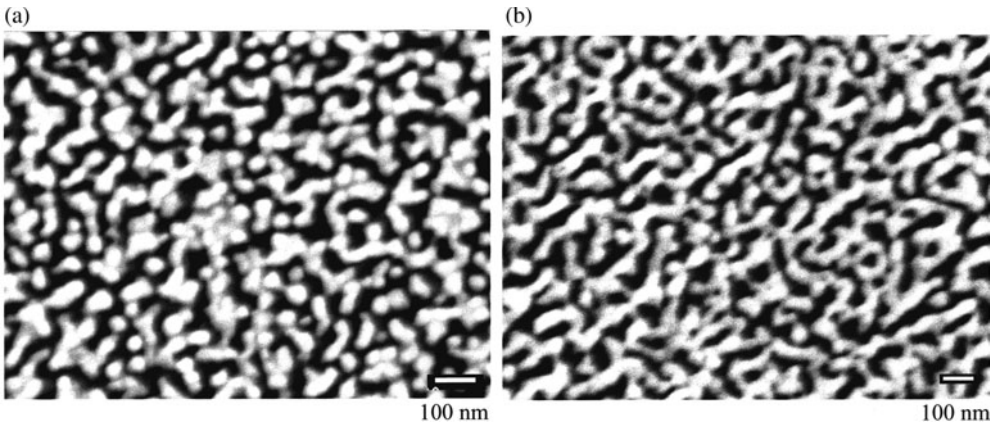

Figure 9. Two SEM images of Ag nanostructures with different AgO_x film thicknesses. (a) 50 nm and (b) 100 nm. The substrates were Si.

Figure 9 shows a typical Ag nanowired structure on a Si surface. As shown in figure 9, some parts are linked and networked together, but the wire's diameter remains mostly the same at approximately 20–30 nm. It appears that the wire's diameter depends on the quantity of CF_4 used for activation. If the CF_4 quantity is large, the diameter is wider. Very recently, we have succeeded in controlling the wire's diameter by changing the gas ratio of CF_4. As first reported [37], the deoxidized pressure was fixed at a constant 10 Pa. With further reduction of the pressure to less than 1.5 Pa, a gas mixture of H_2, O_2 and CF_4 becomes usable for nuclear formation. A typical procedure for a much easier and more promising technique for producing Ag nanostructures is as follows.

(1) Prepare an AgO_x thin film by the reactive sputtering method with an Ag target and gas mixture of Ar and O_2.
(2) After flushing the reactive-ion-etching (RIE) chamber once, put the AgO_x sample in the chamber and evacuate it to below 8×10^{-3} Pa.
(3) Introduce a gas mixture of H_2, O_2 and CF_4, with respective gas ratios of 3, 1 and 0.2.
(4) Maintain the total pressure at 1.5 Pa, and inject RF power of 50 W (note that the power will vary according to chamber size).
(5) Set the deoxidation time to 1.5 min.
(6) Shut down only the CF_4 gas flow, and continue deoxidation for between 1.5 and 5 min with only the gas mixture of H_2 and O_2. (Here, the continuing time depends on the size of the sample.)

The Ag nanostructured layer can also be produced on an Ag metal surface. Figure 10 shows photos of the sample surface. The nanostructured surface appears gold, but the opposite surface is the colour of Ag metal (figures 10(a) and (b)). In comparison, the surface of the as-deposited AgO_x (100 nm) on an Ag metal layer (100 nm thick) is green. Of course, the Ag nanostructured layer, as well as the AgO_x layer, can show SERS activity. One of the problems with SERS observation using AgO_x layers is that as the layer is gradually photothermally decomposed into Ag nanoparticles and wires under a focused laser beam, the intensity and sensitivity of the target chemical gradually changes and intensifies with the elapse of time. Instead, on the Ag nanostructured layer the wire's diameter and dimension are rigidly held; they change only little and remain stable. Figure 11 shows the time dependence of the SERS

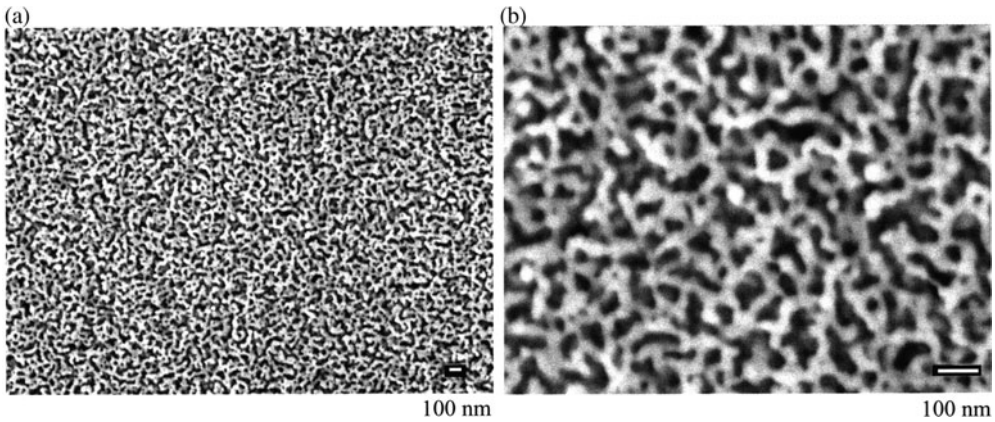

Figure 10. (a) Ag nanowires fabricated on a 100 nm thick Ag layer. The AgO_x layer thickness was 100 nm. Three-dimensional Ag nanowires and their networks are clearly observed. (b) Enlarged image.

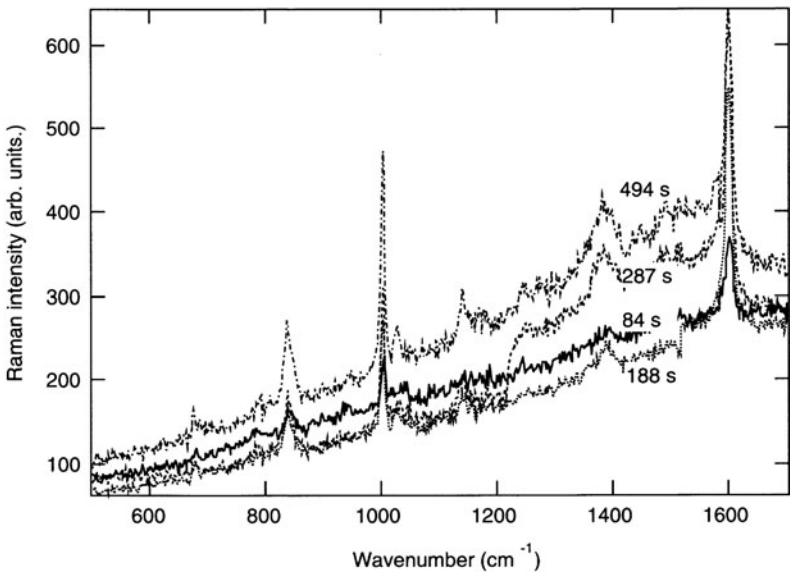

Figure 11. SERS spectra of BA in 2-propanol solution (10^{-3} M) against laser irradiation time, at 84, 188, 287 and 494 s, respectively.

spectrum of BA in 2-propanol. In comparison with the SERS from the AgO_x layer, the spectra from the Ag nanostructured layer remained very stable, even during extended measurement.

Shown in figure 12 (a) are Ag nanowires generated on a high-density pit plastic substrate with a diameter of 12 cm. The AgO_x layer deposited on the disc surface was transformed into the wires in the same manner as mentioned above for 1.5 min. Amazingly, nanostructures were also formed in 200 nm sized pits. Figure 12(b) shows a SEM image of a nanoparticle-covered structure. Hence, an active film ($Ge_2Sb_2Te_5$ alloy of thickness 20 nm) for a DVD-recordable disc was covered with an Ag nanoparticle structure (each diameter: 10 nm). It is clearly shown that the covered particle size is very uniform at approximately 40–50 nm.

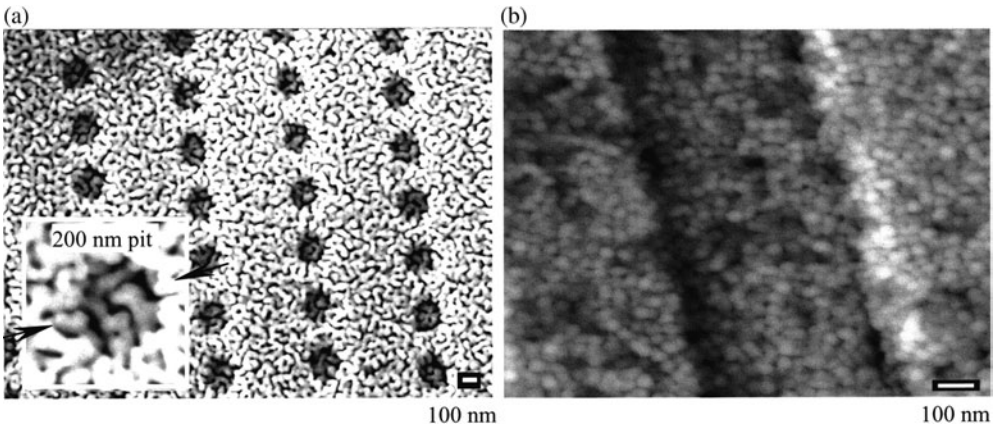

Figure 12. Several examples with the Ag nanoparticles and nanowires. (a) Ag nanowires fabricated on a high-density optical disc. Each pit size is 200 nm. Inset is the expanded image. (b) Patterned GeSbTe phase-change film deposited on the layer covered with Ag nanoparticles (each diameter: 15–20 nm). The particle pattern corresponds to a storage density of more than 400 Gbit in^{-2}.

Since the particle size and distance can be controlled from 10 to 50 nm, a strong optical antenna effect due to *LSP* is expected [38, 39]. Therefore, the nanostructured layer has great potential for future optical nonlinear films and local plasmon devices.

5. Light-scattering centre and overcoming the optical diffraction limit for information data storage

The application of AgO_x thin layers as a recording material for optical data storage was investigated in the early 1990s [29, 30]. The principle of this form of recording was to use thermal decomposition of the film for producing an oxygen pit in the disc medium. As known in chemistry, AgO_x decomposes into Ag and oxygen at above 160 °C at atmospheric pressure. If a thin layer is deposited on a plastic substrate and covered with a hard material such as a SiO_2 or SiN layer, the decomposition pressure and heat are anisotropically focused on the soft surface of the plastic substrate, leaving an oxygen hole or pit at the interface between the substrate and hard coated layer, but with minimal volume deformation. Although the actual procedures for data recording and reproducing the signals are in fact more complex, in combination with a phase difference reflection layer placed behind the hard layer, the disc was able to reproduce recorded pits using a conventional CD drive [29]. A second application of an AgO_x layer to data storage was again carried out in 2000 to enhance the faint data signals of small recorded marks, whose sizes were smaller than the optical diffraction limit: it is now called a *'super-resolution near-field structure (super-RENS)'* [31]. Super-RENS was first developed in 1998 to resolve small signals beyond the optical diffraction limit using a combination of optical super-resolution for optical data storage and a SNOM [40].

Here we briefly explain the principle of the super-RENS and its optical readout. In optical data storage, the minimum recorded and readout mark size is normally determined on the basis of far-field optics, i.e. the optical diffraction limit. The limit d is rigidly determined by the relationship between the incident laser beam wavelength λ and lens numerical aperture NA focusing the beam, expressed as $d = \lambda/2/\mathrm{NA}$. The readable minimum mark size s is half of d: $d = \lambda/4/\mathrm{NA}$, since d is the resolution between two small objectives, in this case pits, and the conditions in the focused laser spot allow both pit and space to be included. In smaller

mark conditions beyond the limit, two pits come into the laser spot, resulting in no signal output. In the latest and most advanced DVD technology using a 405 nm blue laser source and high-NA lens of 0.85, the minimum mark or pit size is limited to around 150 nm. The storage density of a DVD system is thus less than 30 GB for a 12 cm disc. In order to overcome the diffraction limit of far-field optics and to push up the storage density beyond 100 GB or even towards 1 TB, the use of the optical near-field has been studied for the last decade [41–50]. In early research, a SNOM was very often utilized to generate near-field light, whose extension was limited by the aperture size of the SNOM head, but 60 nm size magneto-optical pits were successfully recorded by Betzig *et al* [41, 42]. Following this pioneering work in *near-field recording (NFR)*, several NFR technologies have since been proposed and demonstrated. They are now classified into three methods. One is to use a flying optical small aperture in combination with hard-disk technology [44, 45]; the second is to use a *solid immersion lens (SIL)* (*hemispherical lens*) [43, 46–50]; the third is to apply an optical nonlinear mask layer [30, 31, 40]. The former two methods are based on the principle of SNOM-NFR, in which the generator of near-field photons is installed in the recording and readout head. As was explained in section 1, SP and optical near-field, in principle, are non-propagating electric fields towards space but isolated at the surface or interface with another medium. Therefore, the head needs to be at most 100 nm from the recording medium to obtain a satisfactory *signal to noise ratio (SNR)*. Notably, since the medium needs to rotated faster than 1500 rpm to play back a movie picture, any small shock or turbulence makes the head contact the medium surface, resulting in data crashes. In the third method, on the other hand, the generator of the optical near-field is installed in the recording medium itself by means of an optical nonlinear thin layer placed close to the recording layer. The nonlinear layer and recording layer are separated by a transparent dielectric layer (thickness < 100 nm). The huge advantage of this method is that the near-field generator never touches the recording layer: the medium can be rotated at the same speed or faster than that seen in conventional DVD systems. Plastic substrates can also be used. The near-field photon extension and intensity are hence controlled by the incident laser beam power, since the response of the nonlinear layer depends on the characteristics of the focused beam. The cross section of the super-RENS disc is shown in figure 13. First-generation super-RENS optical discs used an Sb thin film as the nonlinear layer [40], and 60 nm recorded marks were resolved under the readout conditions of a diffraction limit of 550 nm. Although this level of resolution was successfully enabled by the optical near-field effect in first-generation super-RENS, interference caused by the aperture edge interfered with and reduced the signal intensity in the vicinity of 200 nm mark size. In order to improve the super-RENS properties, a second-generation super-RENS disc using a light-scattering centre was proposed in 2000 [30, 31].

Hence, the transparent near-field aperture has been replaced, and the light-scattering part is placed in the actual disc. AgO_x was newly introduced as a replacement for Sb. As has already been discussed, the AgO_x layer decomposes at temperatures above 160 °C, and Ag and oxygen are released. However, as shown in figure 13(b), when the layer is sandwiched between hard materials on both sides, there is no place for the oxygen to escape. This means that a high-pressure area will be produced in the area of the disc on which the laser beam is focused. The AgO_x will partly decompose into Ag particles and oxygen, but soon recombines to form AgO_x again when the laser power is turned off; in fact, it appears that both reversible and irreversible reactions occur in the disc. Along with an increase in the laser beam power for readout, small Ag particles are generated, and strong incident light beams are scattered on the particles, due to the *LSP* effect or the enhanced electrical field. Figure 14 shows typical readout characteristics for a second-generation super-RENS optical disc. The disc can resolve approximately 100 nm mark sizes under the diffraction limit of 550 nm.

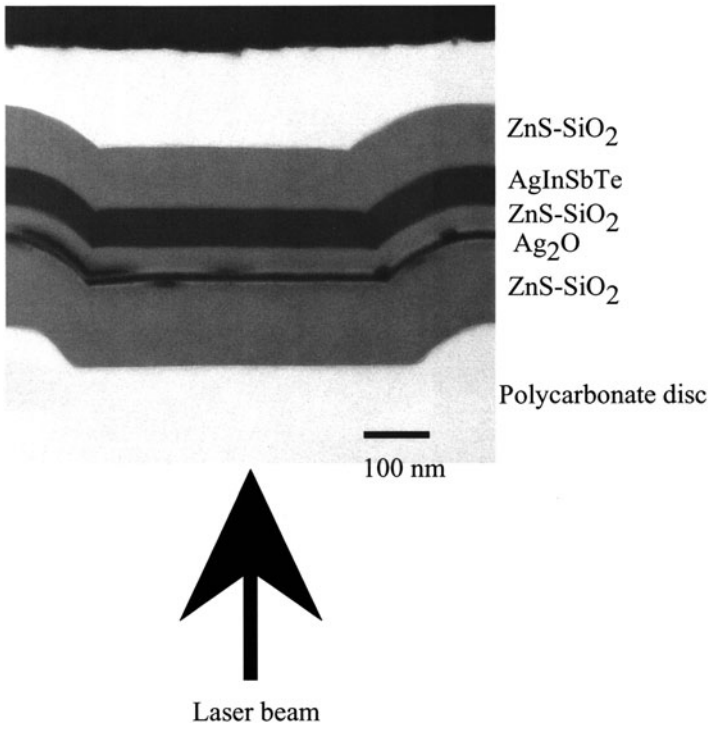

Figure 13. Cross-sectional image taken using transmission electron microscopy of second-generation super-RENS disc. Top $ZnS–SiO_2$ layer (100 nm)/AgInSbTe (60 nm)/intermediate $ZnS–SiO_2$ (40 nm)/AgO_x (15 nm)/bottom $ZnS–SiO_2$ (130 nm).

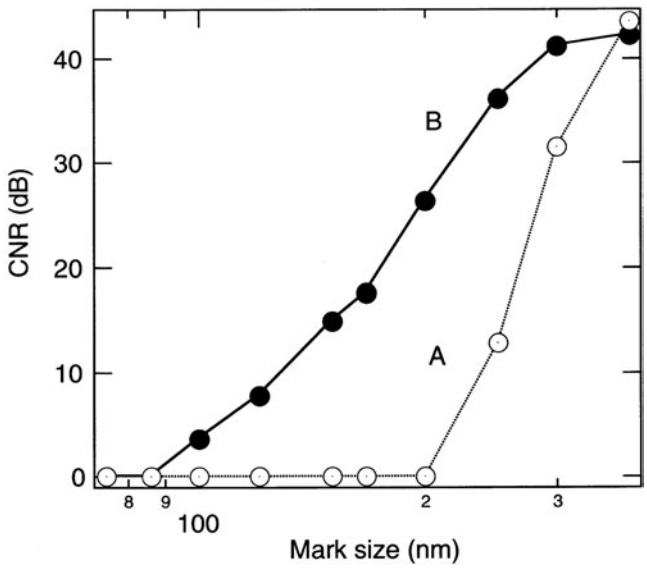

Figure 14. Resolution characteristics of second-generation super-RENS disc. (a) Readout at laser power of 1.5 mW, and (b) readout at 3.5 mW [51].

In comparison with the features of the Sb super-RENS disc, the resolution intensity compared with the mark size is a simple linear function of its size. More recently, the AgO_x layer has been replaced with a platinum oxide (PtOx) layer to further reduce the particle size to less than 20 nm (this is called a third-generation super-RENS disc) [52]. In the third-generation disc, the resolution has been further improved by 50 nm. In this disc, the gas bubble produced by the thermal decomposition of the PtOx film is actively used to generate uniform small metallic nanoparticles. The signal intensity is markedly improved, with a good carrier to noise ratio (CNR): the CNR of 200 nm mark trains was 46 dB under the diffraction limit of 550 nm, and the CNR of 100 nm mark trains reached 40 dB under the diffraction limit of 310 nm. The intensity levels are now approaching practical figures (50 dB) for commercially available optical data storage. A key technology for further increasing the intensity and ensuring better stability of the disc (the relationship between the particle size ϕ and each space δ) is very important. As Remacle *et al* [53] reported, the optical nonlinearity reaches its maximum at approximately $\delta/\phi = 1.2$. Although the value may shift due to changes in the refractive index of the particle and that of the surrounding medium, the value should be tuned to the wavelength with which the medium is irradiated. Once controlled by use of Ag nanoparticles and the wire fabrication technique we mentioned above, super-RENS and NFR using nanometre sized photons will be able to be commercialized in future.

6. Localized plasmon switch and amplification

Through second- and third-generation super-RENS optical disc studies, we have learned a great deal about the properties of nonlinear light-scattering and *LSP*. As discussed in the super-RENS optical disc and high resolution beyond the diffraction limit sections above, light-scattering centres, especially smaller than the wavelength and their scattering natures, have long been of interest in Rayleigh scattering and Mie scattering [54, 55]. Now, when focusing our attention on the recorded pits or marks whose sizes are smaller than the wavelength, the same type of light scattering will be expected in developments such as super-RENS optical discs. Hence in the disc, two different forms of light-scattering occur: light-scattering by small Ag particles, and by the pits or marks recorded in the recorded layer such as an optical phase change layer. In the phase change layer, the recorded mark and non-recorded area have different refractive indices depending on the structural differences between amorphous and crystalline materials [56]. A large refractive index is very suitable for creating a large contrast in near-field properties and enhancing it. Although typical materials for phase-change recording which are now available for recordable DVD discs are $Ge_2Sb_2Te_5$ and $Ag_{11}In_4Sb_{58}Te_{27}$, both dielectric constants of the crystalline states: $-7.76 + 35.19i$ and $-3.18 + 13.86i$ are negative. These constants are very useful for generating SPs as discussed in section 1. In order to generate SPs, an optical grating plays a role, as well as the use of Kretschman geometry. Therefore, crystalline mark trains buried in the amorphous layer may function as optical gratings. As the mark pitch becomes shorter and shrinks to smaller than the wavelength, the layer cannot diffract incident light, after which SPs are generated. In this section, firstly light-transmittance characteristics by two close light-scattering centres are discussed [57], followed by light amplification with a super-RENS disc [58].

Figure 15 shows a cross-sectional image of our test disc. The recording layer is removed and replaced with a second AgO_x layer. Several test discs with different intermediate layer thicknesses between two AgO_x layers were prepared. Using two laser pickup sources with photodetectors and employing DVD drive technology, two focused laser beams can be crossed on the test disc which is rotating at high speed (6.0 m s^{-1} at constant linear velocity). The two beams are focused from different directions along the same axis. To measure the light

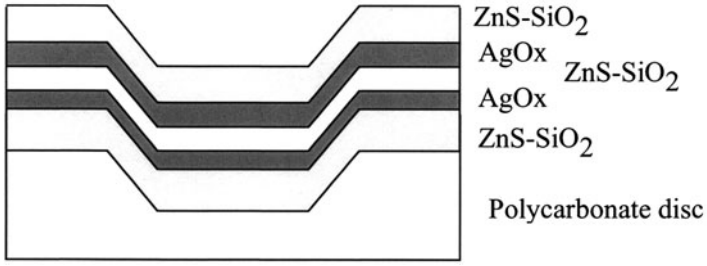

Figure 15. Schematic picture of cross section of a double AgO_x super-RENS disc. AgO_x film thicknesses are both 20 nm.

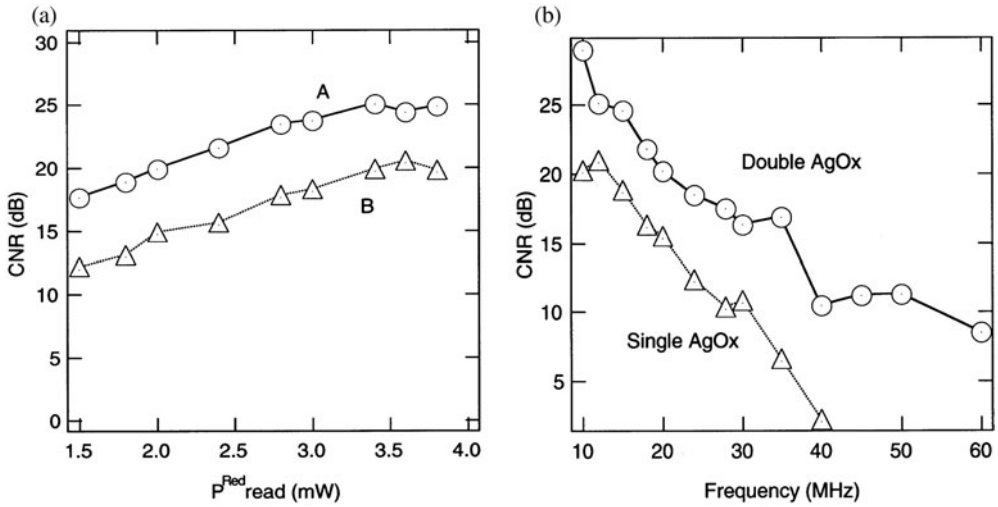

Figure 16. Modulated laser (405 nm wavelength) signal detection in transmission mode against DC laser (635 nm wavelength) power intensity. The intermediate ZnS–SiO_2 film thickness was 20 nm. The disc was rotated at a constant linear velocity of 6.0 m s^{-1}. (a) Single-carrier intensity against DC laser power; A, 405 nm laser modulation between 1.0 and 1.5 mW; B, between 1.0 and 1.1 mW. Modulated frequency was 15 MHz. (b) Frequency response from the double structure and a single AgO_x structure at a DC laser power of 3.8 mW.

transmitted from the disc, one laser beam is power modulated between 1.0 and 1.5 mW, which does not generate Ag particles in the discs. The other beam is not modulated, but is only used to generate and eliminate the scattering centres with DC power change. The variations of transmitted light intensities of the discs are shown in figure 16.

As shown in figure 16(a), the transmitted signal intensity depends on the DC-laser power intensity. This means that the DC power generates light-scattering centres in the AgO_x layers, resulting in enhanced signal intensity. In figure 16(b), on the other hand, the scattering signal intensity with the double AgO_x layers is higher than that with a single AgO_x layer, although the light transmittance is decreased by the light absorption from the second AgO_x layer. This result is evidence that *LSP* coupling in fact occurs between both AgO_x layers. The real observed signal, detected using a spectrum analyser, is shown in figure 17. At around the second transition, a relatively large transmittance change is observed as a result of a reduction in the thickness of the intermediate layer (figure 18). It is also noticeable that there is another high-transmittance point at $d = 0.25$ (where the thickness of the intermediate ZnS–SiO_2 film

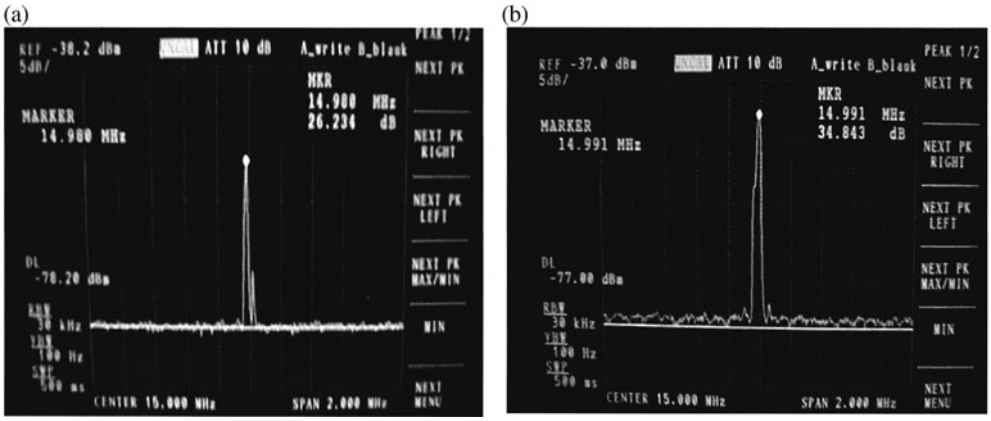

Figure 17. Transmitted signals observed by spectrum analyser. The modulated laser power in this case was between 1.0 and 4.5 mW. (a) DC laser power was 1.5 mW and (b) 3.5 mW [57].

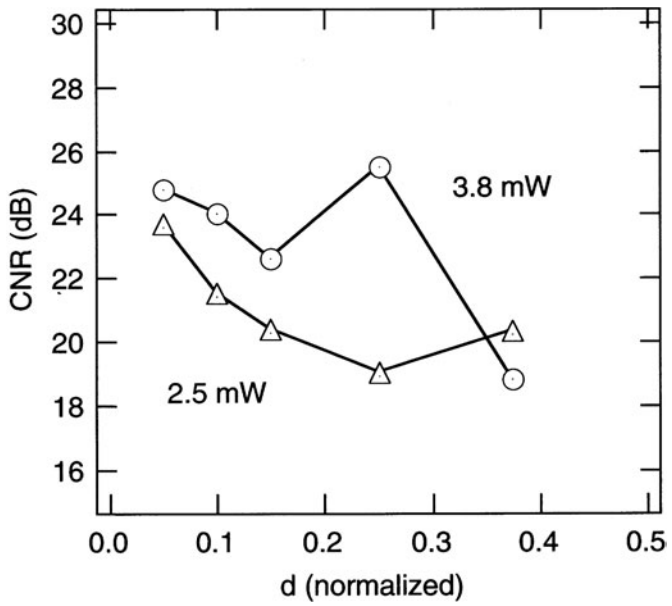

Figure 18. Single-carrier intensity dependence on the intermediate ZnS–SiO_2-film thickness (normalized by 405 nm wavelength) at DC laser powers of 2.5 and 3.8 mW. The modulation frequency was 15 MHz [57].

is 100 nm). This thickness value coincides with the half wavelength of the power-modulated laser beam (405 nm) due to the layer's refractive index being 2.1. This is likely to be the first resonance cavity point of the far-field wave. On the other hand, the transmitted light increment of less than 50 nm is hard to explain using only far-field optics, since the nature of the optics is gradually dominated by near-field or *LSP* coupling. The results also provide strong evidence that small Ag particles placed close to one another at a range of several tens of nanometres are able to control light energy and work well as a photonic switch. One of the disadvantages of the test device is that the switch has to be rotated at a relatively high speed, otherwise the

accumulated light energy rapidly destroys the multilayer structure. Therefore, in order to use such a photonic device in stationary fashion, Ag particles need to be formed or fabricated from the beginning. The Ag nanoparticles and wires discussed in the early section will be of great help in fabricating a static photonic switch and reducing heat build-up.

Double-AgO_x-layer studies have revealed that with two focused laser beams, small Ag particles can function as light-couplers and photonic switches. On the other hand, periodic mark trains consisting of small crystals in the phase-change recording layer play the role of another light-scattering centre. There exists a simple relationship between the grating pitch a and diffraction angle θ.

$$k_x = \omega/c \sin\theta \pm \nu g. \tag{3}$$

Here, $g = 2\pi/a$ and ν is an integer. Therefore, if the mark pitch or mark length changes, the wavevector component along the layer surface also changes; the nature of the SP and its energy can be controlled. That is, in each track with a different recorded mark size or pitch in the light-scattering super-RENS disc, the transmitted or reflected light intensity may be changed by increasing or decreasing the intensity of the light-scattering centre in the AgO_x layer. We recently confirmed that it was possible to control SPs and to transfer the energy to far-field light by placing the Ag light-scattering centre in the super-RENS disc [57]. Using the same system as employed in *LSP* switches, two laser beams were focused on the disc from the opposite direction. Hence, although we used two different wavelength laser sources, they should be the same wavelength to hopefully obtain higher gains. As shown in figure 19, one laser source (in this case with a wavelength of 405 nm) was power modulated with a small total power, which is not enough to generate a scattering centre in the AgO_x layer as well as the plasmon photonic switch. The power of the other laser (in this case with a wavelength of 635 nm) was continuously controlled to increase or decrease the function of the light-scattering centre in the layer. Hence, it is clear that a focused DC laser can also generate SPs due to the recorded mark patterns. SPs were then also scattered by the scattering centre.

Therefore, the photodetector installed in the DC laser pickup unit observes two different signals: the frequency signal due to the light-scattering generated by the recorded periodic pattern, and the power-modulated frequency of the transmitted light of the second laser source. For example, if a frequency of 15 MHz is recorded with a duty ratio of 0.5 on the disc at a constant linear velocity of 6.0 m s^{-1}, the recorded mark size and spaces will each be 200 nm in length. It should be understood that the recording mark size is not determined by the resolution limit, since the phase-change transition in the recording layer responds to the temperature profile produced by the laser intensity's profile. Therefore, by controlling the power and cooling speed on the produced mark, in principle, marks shorter than 100 nm can be recorded and have in fact been confirmed [40]. The pattern size is smaller than that of the resolution limit of the DC laser pickup unit, but somewhat larger than the limit size of the power-modulated laser unit. Therefore, under normal readout conditions, the detector in the DC laser pickup unit cannot resolve the recorded signal; only the transmitted signal of the second source (405 nm) is detected. On the other hand, a detector installed in the second source (power-modulated source) can detect both reflected signals of the recorded mark frequency and the modulated signal itself. Hence, the respective resolution limits of the pickup systems are 270 and 150 nm. If the two laser beams are crossed at the position on the same track where the periodic small mark pattern has been recorded, when the laser power is small (1.0 mW), the detector in the DC laser unit detects only the modulated signal from the second laser source. With increasing DC laser power, the light-scattering centre is gradually generated, and as a result the detector gradually gains the ability to detect a second signal: the signal due to the mark pattern recorded in the disc using the modulated source signal. As the DC laser power is further increased, the

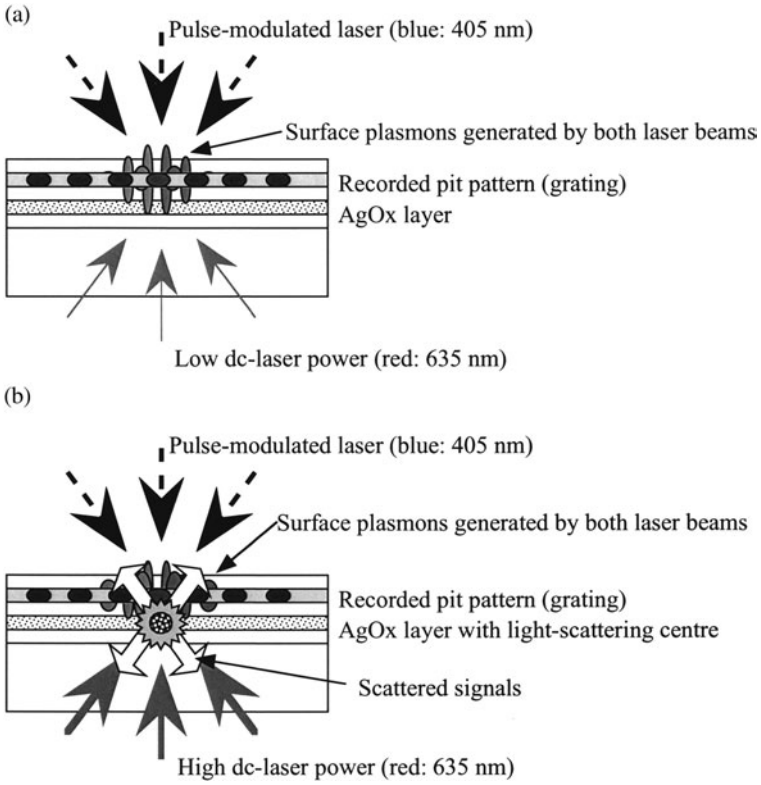

Figure 19. Principle of local plasmon photonic transistor. If DC laser power is low, no scattering centre is generated in the AgO_x layer and the SP is simply trapped at the interface between the recording film and the dielectric film (a). As the power is increased, light-scattering is generated and the size grows. Light-coupling occurs between the scattering centre and trapped SP, as has been shown in the plasmon photonic switch. The trapped SP signals are then retrieved as far-field light. In the experiment, two laser sources with different wavelengths are used to eliminate the interference that would be caused by the reflected DC laser beam.

modulated signal intensity is gradually enhanced along with the intensity of the second peak. The second intensity effect is a normal enhancement observed in the super-RENS disc. This is called *self-amplification*. Figure 20 shows the gain with and without the recorded mark pattern. 0 mW indicates that no mark pattern is recorded on the disc. The gain is small at less than 2 dB, which would depend only on the light-scattering centre. 6.0 mW indicates the threshold: the minimum power for mark recording on the disc. With increasing power, the mark pattern is uniformly recorded in the track. As shown in figure 20, the gain at the recording power of 7 and 8 mW reaches more than 10 dB, when increasing the DC laser power intensity by 2.0 mW. The mark pattern pitch also affects the gain intensity. Figure 21 shows the relationship between the maximum gain and mark size (half of the pitch). The smaller the mark size, the more gain is observed. The results strongly suggest that the diffracted light energy as SP is actually accumulated over several marks and spaces in the laser spot areas. There, SP energy is released and scattered outside the disc due to light-coupling between the SPs due to the pattern and the *LSPs* around the scattering centre. Even with two different wavelengths, the fact that enhancement was observed is very interesting and promising, because SPs are generated by the motion of electrons in a medium with a negative dielectric constant. It is assumed that the

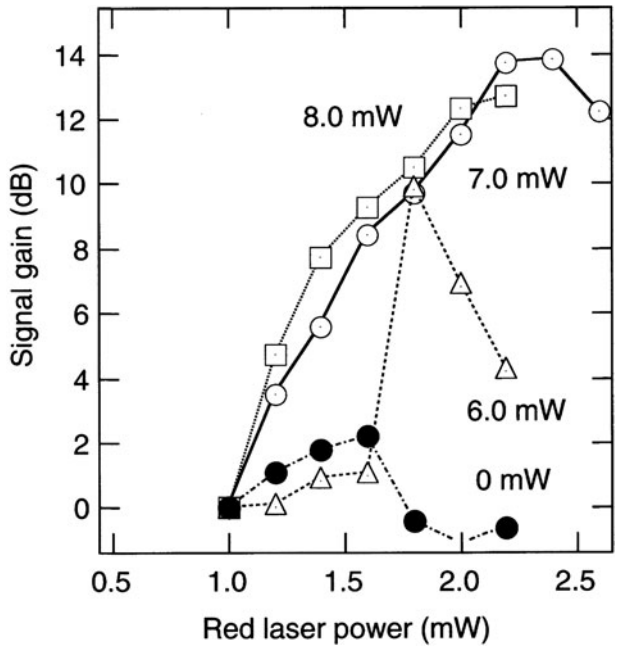

Figure 20. Single-carrier gain observed in local plasmon photonic transistor. 200 nm mark trains were recorded on the second-generation super-RENS disc. The modulation laser frequency was 15.3 MHz with power varied between 0.5 and 0.7 mW. 0 mW indicates that no recording took place. The disc was rotated at a constant linear velocity of 6.0 m s^{-1} [57].

optical nonlinearities of the phase-change layer and nanometre-size Ag particles are large. We expect that the detailed characteristics will be confirmed in a stationary state by using the Ag nanoparticles and nanowires described in this paper in the near future.

7. Summary

We have described the unique characteristics of AgO_x layers, and their application to photonic devices using surface plasmons and *LSP*. Although AgO_x is not a new material, it is easy to handle and can be deposited on almost any material surface by vacuum deposition, especially by sputtering. The deposited layer can be transformed into Ag nanoparticles and nanowires in a gas mixture of H_2 and O_2. The diameter and space between each wire or particle can also be controlled over a limited range by feeding a seed gas before or during the reduction process. Once this method is applied and combined with integrated circuit production, these particles and wires will be able to be applied on a nanometre scale as point-to-point connectors or pinpoint light emitters. On the other hand, in recent advanced optics, photonic crystals have attracted a great deal of attention, since they will open the way to reducing the size of optical components. Silver nanoparticles and wires will be also used for transferring photons from one waveguide to another as localized plasmons. For optical data storage, the material has long been examined and studied for potential applications, first in recordable CDs, and then in super-resolution high-density discs using near-field optics, although AgO_x has not been the main recording source. It is clear, though, that in future this material will play an important role in near-field optics and surface plasmon engineering, as well as in advanced optical storage.

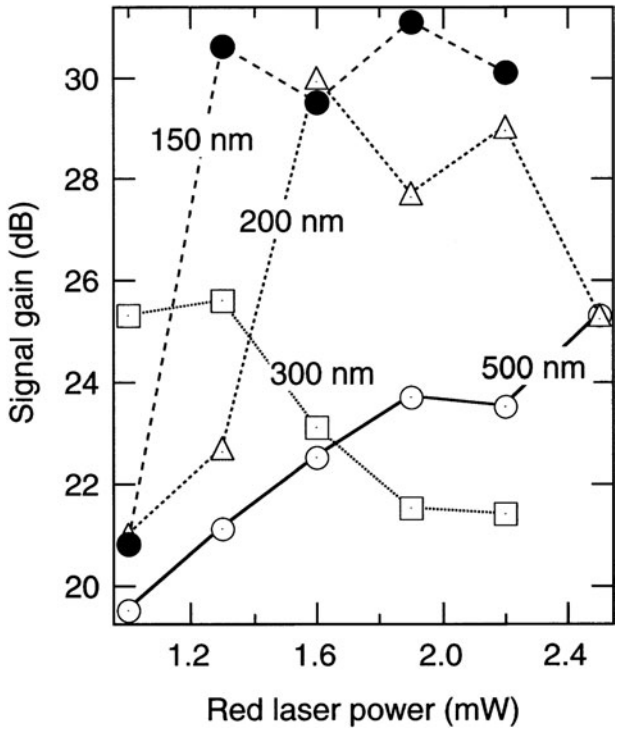

Figure 21. Single-carrier gain dependence on recorded mark train size. The mark recording power was 7.0 mW, and the signals were observed at a modulation frequency of 14.8 MHz [57].

Acknowledgments

The author wishes to thank T Fukaya, T Nakano, M Kuwahara and T Shima at Laotech, and our former colleagues D Büchel and C Mihalcea (now both at Seagate Technology, USA), and J H Kim of Samsung Electronics, T Kikukawa of TDK Corporation and H Fuji of Sharp Company particularly for super-RENS disc development.

References

[1] Liu W-G, Wu H, Xiong Y-Q, Guo Y, Yang D-Q and Li H-L 2000 *J. Vac. Sci. Technol.* B **18** 1156
[2] Weimer W A and Dye M J 2001 *Appl. Phys. Lett.* **79** 3164
[3] Worthing P T and Barnes W L 2001 *Appl. Phys. Lett.* **79** 3035
[4] Went H E and Sambles J R 2001 *Appl. Phys. Lett.* **79** 575
[5] Moskovitz M 1985 *Rev. Mod. Phys.* **57** 783
[6] Chang R K and Futak T P 1982 *Surface-Enhanced Raman Scattering* (New York: Plenum)
[7] Tranenko N, Alarie J-P, Stokes D L and Dinh T V 1996 *J. Raman Spectrosc.* **27** 379
[8] Li Y-S 1994 *J. Raman Spectrosc.* **25** 795
[9] Mou C, Chen D, Wang X, Zhang B, He T, Xin H and Liu F-C 1991 *Chem. Phys. Lett.* **179** 237
[10] Wang X, He T, Wan H, Xu C, Zuo J and Liu F-C 1997 *Spectrochim. Acta* A **53** 1411
[11] Li Y-S, Lin X and Cao Y 1995 *Vib. Spectrosc.* **20** 95
[12] Somekh M G, Liu S, Velinov T S and See C W 2000 *Appl. Opt.* **39** 6279
[13] Jung L S, Nelson K E, Campbell C T, Stayton P S, Yee S S, Perez-Luna V and Lopez G P 1999 *Sensors Actuators* B **54** 137
[14] Ballerstadt R and Scultz J S 1998 *Sensors Actuators* B **46** 50

[15] Nie S and Emory S T 1997 *Science* **275** 1102
[16] Peyser L A, Visnon A E, Bartko A P and Dickson R M 2001 *Science* **291** 103
[17] Exter M and Lagendijk A 1988 *Phys. Rev. Lett.* **60** 49
[18] Raether H 1988 *Surface Plasmons on Smooth and Rough Surfaces and on Gratings* (Berlin: Springer)
[19] Worthing P T and Barnes W L 2001 *Appl. Phys. Lett.* **79** 3035
[20] Went H E and Sambles J R 2001 *Appl. Phys. Lett.* **79** 575
[21] Milner R G and Richards D 2001 *J. Microsc.* **202** 66
[22] Ayars E J and Hallen H D 2000 *Appl. Phys. Lett.* **76** 3911
[23] Inouye Y and Kawata S 1994 *Opt. Lett.* **19** 159
[24] Hayazawa N, Inouye Y and Kawata S 1997 *J. Microsc.* **197** 472
[25] Hayazawa N, Inouye Y, Sekkat Z and Kawata S 2001 *Chem. Phys. Lett.* **335** 369
[26] Novotony L, Pohl D W and Regli P 1994 *J. Opt. Soc. Am.* A **11** 1768
[27] Ferber J, Fischer U C, Hagedorn N and Fuchs H 1999 *Appl. Phys.* A **69** 581
[28] Tominaga J, Haratani S, Uchiyama K and Takayama S 1992 *Japan. J. Appl. Phys.* **31** 2757
[29] Haratani S, Tominaga J, Dohi H and Takayama S 1994 *J. Appl. Phys.* **76** 1297
[30] Tominaga J, Büchel D, Nakano T, Fuji H, Fukaya T and Atoda N 2000 *Proc. SPIE* **4081** 86
[31] Fuji H, Tominaga J, Men L, Nakano T, Katayama H and Atoda N 2000 *Japan. J. Appl. Phys.* **39** 980
[32] Schmidt A A, Offermann J and Anton R 1996 *Thin Solid Films* **281/282** 105
[33] Buechel D, Tominaga J, Fukaya T and Atoda N 2001 *J. Magn. Soc. Japan* **25** 240
[34] Fukaya T, Büchel D, Shinbori S, Tominaga J, Atoda N, Tsai D P and Lin W C 2001 *J. Appl. Phys.* **89** 6139
[35] Büchel D, Mihalcea C, Fukaya T, Atoda N, Tominaga J, Kikukawa T and Fuji H 2001 *Appl. Phys. Lett.* **79** 620
[36] Mihalcea C, Büchel D, Atoda N and Tominaga J 2001 *J. Am. Chem. Soc* **123** 7172
[37] Tominaga J, Shima T and Kuwahara M 2002 *Abstract of Micro– and Nano–engineering International Conference, Lugano, Switzerland 16–19 September 2002*
[38] Kottmann J P and Martin O J F 2001 *Opt. Lett.* **26** 1096
[39] Setala T, Kaivola M and Friberg A T 2001 *J. Opt. Soc. Am.* A **18** 678
[40] Tominaga J, Nakano T and Atoda N 1998 *Appl. Phys. Lett.* **73** 2078
[41] Betzig E, Trautman J K, Wolfe R, Gyorgy E M, Finn P L, Kryder M H and Chang C H 1992 *Appl. Phys. Lett.* **61** 142
[42] Betzig E, Grubb S G, Chichester R J, DiGiovanni D J and Weiner J S 1993 *Appl. Phys. Lett.* **63** 3550
[43] Terris B D, Mamin H J, Rugar D, Studenmund W R and Kino G S 1994 *Appl. Phys. Lett.* **65** 388
[44] Ukita H, Katagiri Y and Nakada H 1991 *SPIE* **1449** 248
[45] Yoshikawa H, Ohkubo T, Fukuzawa K, Bouet L and Yamamoto M 1999 *Appl. Opt.* **38** 863
[46] Terris B D, Mamin H J and Rugar D 1996 *Appl. Phys. Lett.* **68** 141
[47] Ichimura I, Hayashi S and Kino G S 1997 *Appl. Opt.* **36** 4339
[48] Mansfield S M and Kino G S 1990 *Appl. Phys. Lett.* **57** 2615
[49] Yeh W and Mansuripur M 2000 *Appl. Opt.* **39** 302
[50] Kasami Y, Yasuda K, Ono M, Fukumoto A and Kaneko M 1996 *Japan. J. Appl. Phys.* **35** 423
[51] Tominaga J, Kim J H, Fuji H, Büchel D, Kikukawa T, Men L, Fukuda H, Sato A, Nakano T, Tachibana A, Yamakawa Y, Kumagai M, Fukaya T and Atoda N 2001 *Japan. J. Appl. Phys.* **40** 1831
[52] Kikukawa T, Nakano T, Shima T and Tominaga J 2002 *Appl. Phys. Lett.* **81** 4697
[53] Remacle F, Collier C P, Heath J R and Levine R D 1998 *Chem. Phys. Lett.* **291** 453
[54] Born M and Wolf E 1999 *Principles of Optics* 7th edn (Cambridge: Cambridge University Press)
[55] Atkins P W 2000 *Physical Chemistry* 6th edn (Oxford: Oxford University Press)
[56] Yamano N and Mitsunaga T 2000 *J. Appl. Phys.* **88** 7020
[57] Tominaga J and Tsai D P 2003 *Optical Nanotechnologies—the Manipulation of Surface and Local Plasmons* (Heidelberg: Springer)
[58] Tominaga J, Mihalcea C, Büchel D, Fukuda H, Nakano T, Atoda N, Fuji H and Kikukawa T 2001 *Appl. Phys. Lett.* **78** 2417